



MYC controls STING levels to downregulate inflammatory signaling in breast cancer cells upon DNA damage

Received for publication, October 11, 2024, and in revised form, April 22, 2025. Published, Papers in Press, April 29, 2025.
<https://doi.org/10.1016/j.jbc.2025.108560>

Renske Linstra¹ , Chantal Stappenbelt¹, Femke J. Bakker¹ , Marieke Everts¹ , Arkajyoti Bhattacharya¹ , Shibo Yu², Stella D. van Bergen¹, Bert van der Vegt² , G. Bea A. Wisman³ , Rudolf S. N. Fehrmann¹, Marco de Bruyn³, and Marcel A. T. M. van Vugt^{1,*}

From the ¹Department of Medical Oncology, University Medical Center Groningen, University of Groningen, Groningen, The Netherlands; ²Department of Pathology and Medical Biology, University of Groningen, University Medical Center Groningen, Groningen, The Netherlands; ³Department of Obstetrics and Gynecology, University of Groningen, University Medical Center Groningen, Groningen, The Netherlands

Reviewed by members of the JBC Editorial Board. Edited by Paul Shapiro

Amplification of the *MYC* proto-oncogene is frequently observed in various cancer types, including triple-negative breast cancer (TNBC). Emerging evidence suggests that suppression of local antitumor immune responses by *MYC*, at least in part, explains the tumor-promoting effects of *MYC*. Specifically, *MYC* upregulation was demonstrated to suppress the tumor-cell intrinsic activation of a type I interferon response and thereby hamper innate inflammatory signaling, which may contribute to the disappointing response to immunotherapy in patients with TNBC. In this study, we show that *MYC* interferes with protein expression and functionality of the STING pathway. *MYC*-mediated STING downregulation in BT-549 and MDA-MB-231 TNBC cell lines requires the DNA-binding ability of *MYC* and is independent of binding of *MYC* to its co-repressor MIZ1. Both STAT1 and STAT3 promote the steady-state expression levels of STING, and STAT3 cooperates with *MYC* in regulating STING. Conversely, *MYC*-mediated downregulation of STING affects protein levels of STAT1 and downstream chemokine production. Furthermore, we show that *MYC* overexpression hampers immune cell activation triggered by DNA damage through etoposide or irradiation treatment and specifically impedes the activation of natural killer cells. Collectively, these results show that *MYC* controls STING levels and thereby regulates tumor cell-intrinsic inflammatory signaling. These results contribute to our understanding of how *MYC* suppresses inflammatory signaling in TNBC and may explain why a large fraction of patients with TNBC do not benefit from immunotherapy.

Triple-negative breast cancer (TNBC) accounts for 15 to 20% of all breast cancer cases and is associated with an increased likelihood of distant recurrence and mortality when compared to other types of breast cancer (1). TNBCs lack expression of the ER, PR, and HER2 receptors and are characterized by elevated levels of genomic instability (2, 3). The current standard-of-care for patients with TNBC involves

radiotherapy and chemotherapy (4). Due to their high level of genomic instability, TNBCs would be expected to be highly immunogenic (5, 6), and as a consequence thereof, TNBCs were expected to respond favorably to immune checkpoint inhibitor treatment (5). While immunotherapy holds significant promise for the treatment of TNBC, reported response rates to single-agent immune checkpoint inhibition are limited, while favorable responses were observed to combined immune checkpoint inhibition with chemotherapy in a subset of patients (7, 8). Clearly, there is substantial opportunity for further advancement of immune checkpoint inhibition in patients with TNBC.

An important factor in driving the response to immune checkpoint inhibitors is interferon (IFN) signaling (9, 10). Genomic instability, either caused by tumor cell-intrinsic factors or caused by DNA damage induced by exogenous sources, such as genotoxic chemotherapeutics, is increasingly recognized to instigate inflammatory signaling (6, 11, 12). Specifically, DNA damage leads to activation of a range of cytoplasmic pattern recognition receptors, including cGAS (*cyclic GMP-AMP synthase*), which recognizes cytoplasmic dsDNA and induces a type I IFN response *via* its adaptor protein STING (*stimulator of interferon genes*) (13–16). Various types of genotoxic treatment were demonstrated to induce cGAS-STING signaling, including irradiation, cisplatin, and hydroxy urea (12, 17). Subsequently, the cytokines and chemokines that are secreted upon DNA damage-induced cGAS-STING activation modify the tumor micro-environment (15) and lead to attraction and activation of immune cells to clear tumor cells. However, TNBCs have apparently evolved mechanisms to escape clearance by the immune system, which counteracts treatment efficacy.

TNBCs are characterized by extensive amounts of genomic alterations (18, 19). A particular recurrent genomic alteration involves focal amplification of the *MYC* proto-oncogene, which affects approximately 15 to 40% of all TNBCs (20–23). *MYC* is a transcriptional regulator, which interacts with MAX to form the *MYC*-MAX complex that drives transcriptional activation of a large group of target genes

* For correspondence: Marcel A. T. M. van Vugt, m.vugt@umcg.nl.

MYC suppresses STING expression

(24–26). Conversely, when the MYC–MAX complex is bound to the transcription repressor MIZ1, MYC can suppress the expression of target genes (27, 28).

MYC is a known driver oncogene in a range of tumor subtypes (29). Increasing evidence suggests that part of the tumor-promoting effects of MYC involves the suppression of local antitumor immune responses (30). For example, overexpression of MYC in a mouse model of lung adenocarcinoma caused reprogramming of surrounding stromal cells and resulted in the attraction of immune-suppressive and tumor-promoting immune cells (31). A similar pattern was observed in a mouse model of pancreatic ductal adenocarcinoma, in which MYC overexpression resulted in an immune-suppressive tumor microenvironment, involving the loss of intratumoral CD3+ T cells (32). Moreover, MYC has been found to directly suppress genes associated with the type I IFN pathway in a MIZ1-dependent manner in both pancreatic ductal adenocarcinoma and TNBC models, leading to reduced infiltration of antitumor immune cells (20, 32, 33). Collectively, these findings indicate that MYC acts as a cancer cell-intrinsic factor that promotes immune evasion of tumors (34). However, how exactly MYC regulates cGAS-STING-IFN signaling remains incompletely clear. In this study, using triple-negative cell lines BT-549 and MDA-MB-231, we show that MYC downregulates STING protein levels and that MYC-mediated suppression of STING leads to a decreased type I IFN response induced by radiotherapy and chemotherapy.

Results

MYC suppresses STING expression at the protein and mRNA level

To determine the effects of MYC overexpression on the abundance of cGAS–STING pathway components, BT-549 TNBC cells with doxycycline (Dox)-inducible overexpression of MYC were analyzed. Whereas the expression of cGAS, IRF3, TBK1 remained unaffected upon MYC overexpression, we observed a notable decrease in the protein abundance of STING and STAT1, which was not observed in Dox-treated control cells (Fig. 1A). Conversely, when MYC expression was decreased using shRNA-mediated MYC depletion in BT-549 cells, the protein levels of STING and STAT1 were significantly increased (Fig. 1B). To investigate whether MYC modulated STING at the transcriptional level, STING mRNA levels were analyzed in a panel of TNBC cell lines (BT-549, HCC-1806, MDA-MB-231) and immortalized epithelial RPE1-*TP53*^{-/-} cells. In line with the observed changes at the STING protein level, MYC overexpression resulted in the downregulation of STING mRNA in all tested cell lines (Fig. 1C). The suppression of STING by MYC was also observed in ER⁺/HER2⁻ MCF7 breast cancer cells (Fig. S1A).

MYC mRNA expression is inversely correlated with STING mRNA expression in multiple cancer types

To analyze whether the observed inverse relation between STING and MYC was also observed in patient samples, we

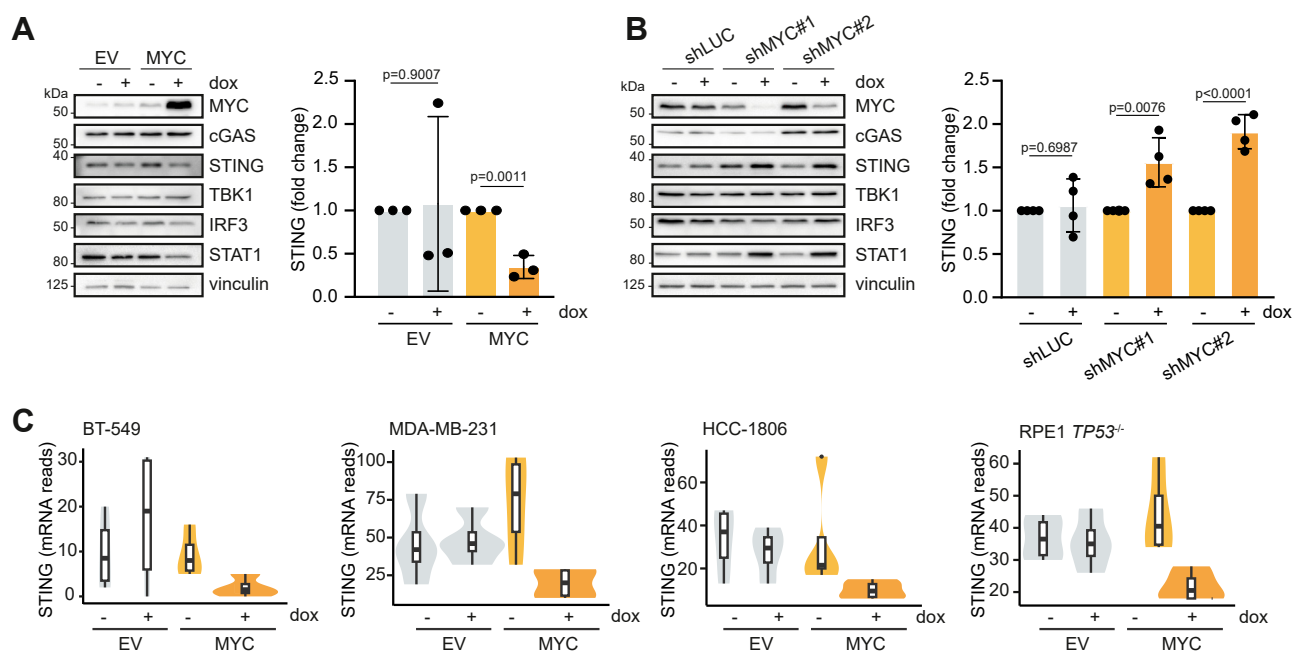


Figure 1. MYC Suppresses STING expression at both protein and mRNA levels and shows an inverse correlation with STING mRNA expression across multiple cancer types. A, BT-549 cells transduced with doxycycline-inducible MYC constructs were treated with doxycycline (10 ng/ml) for 48 hours. Immunoblotting was performed for MYC, cGAS, STING, TBK1, IRF3, STAT1, and vinculin. Molecular weight markers are indicated. Quantification of STING levels from three independent experiments is indicated. *p* values were calculated using an unpaired two-tailed Student's *t* test. Mean and SD are plotted. B, BT-549 cells stably expressing the indicated shRNAs were treated with doxycycline (dox, 1 μg/mL) for 72 h. Immunoblotting was conducted for the indicated proteins. Quantification of STING protein levels from four independent experiments is indicated. *p* values were calculated using an unpaired two-tailed Student's *t* test. Mean and SD are plotted. C, analysis of STING mRNA read counts in BT-549, MDA-MB-231, HCC-1806, and RPE1 *TP53*^{-/-} cell lines expressing doxycycline (dox)-inducible MYC constructs. Cells were treated with doxycycline for 48 h. Violin plots display the data distribution, with box and whiskers indicating the median and interquartile ranges for each condition.

investigated MYC and STING mRNA levels across multiple cancer subtypes, using the TCGA cohort (35). In agreement with our observations in cell line models, MYC mRNA expression was inversely correlated with STING mRNA expression across various cancer types, including breast cancer, and most prominently in gastric adenocarcinoma (Fig. 2A, Table S1). When analyzing the different breast cancer subtypes in the TCGA dataset, MYC amplification showed a statistically significant association with decreased STING mRNA levels in ER⁺/HER2⁻ breast cancers (Fig. 2B, Table S1). Although a trend in inverse correlation between MYC amplification and STING mRNA expression was also observed in other breast cancer subtypes within the TCGA cohort, these did not show statistical significance, likely due to the limited number of samples per breast cancer subtype in our analysis (Fig. 2C). Yet, TNBCs showed the highest percentage of MYC amplification (Fig. 2C). To extend our analysis to a second cohort, we analyzed the METABRIC dataset (36). MYC and STING mRNA levels were inversely correlated, especially in basal-like breast cancers (Fig. 2D), a molecularly defined breast cancer subtype which encompasses the majority of TNBCs. Importantly, MYC mRNA expression was also correlated with decreased immune cell abundance, particularly T cells, B cells, and NK cells, in the tumor microenvironment of HER2⁺ and basal-like breast cancers (Fig. 2D). In line with expectations, STING mRNA was positively correlated with immune cell presence in the tumor microenvironment (Fig. 2E). Similar results were obtained when mRNA levels of MYC and STING were correlated to immune cell composition in TCGA breast cancer samples (Fig. 2, F and G). Because 1) STING downregulation was observed in multiple TNBC cell line models (Fig. 1, A–C), 2) MYC amplification is most frequently observed in TNBCs among breast cancer subtypes, and 3) because the strongest inverse relation between MYC expression and immune cell composition was observed in basal-like breast cancers, we further focused on TNBC models.

Regulation of STING by MYC requires its DNA-binding domain, but is independent of MIZ1

Previous studies revealed that MYC suppresses IFN-related genes in conjunction with the transcriptional repressor MIZ1 (20, 32, 33). We therefore investigated whether MYC regulates STING levels in a similar fashion, using a panel of separation-of-function MYC variants. Specifically, we analyzed MYC^{T58A}, showing increased stability (37, 38), MYC^{V394D}, which cannot interact with MIZ1 and is unable to repress transcription (39, 40), and MYC^{L420P}, which is defective in MAX binding and therefore cannot interact with DNA and cannot regulate transcriptional activation or repression (Fig. 3A) (41). These MYC variants were stably expressed in BT-549 and MDA-MB-231 TNBC cells, followed by the analysis of STING levels. As anticipated, expression of MYC^{WT} and MYC^{T58A} resulted in the downregulation of STING expression in MDA-MB-231 and BT-549 cells (Figs. 3B, and S1, B and C). By contrast, the

introduction of MYC^{L420P} did not lead to downregulation of STING, indicating that the DNA-binding ability of MYC is crucial for suppressing STING levels (Figs. 3B and S1B). Surprisingly, expression of MYC^{V394D} did suppress STING levels, showing that the interaction between MYC and MIZ1 is not required for regulating STING levels and that downregulation of STING by MYC is likely not explained by transcriptional repression by the MYC–MIZ1 complex (Figs. 3B and S1B). In line with these findings, shRNA-mediated depletion of MIZ1 did not lead to increased STING levels (Fig. 3C).

To investigate the effects of the MYC mutants on downstream signaling of STING, a THP-1 cell line with a STING-specific fluorescence reporter (tdTomato) was used, driven by five tandem interferon-stimulated response elements (ISREs) (Fig. 3D) (42). Although THP-1 cells are not of TNBC origin, THP-1 express high levels of STING compared to other cell lines, making THP-1-ISRE-tdTomato cells particularly suitable for analyzing STING signaling at the single cell level (42). STING signaling in these experiments was induced by treatment with the STING agonist MSA2 (43), which resulted in a robust activation of the ISRE reporter (Figs. 3E, S1D). Expression of MYC^{WT}, MYC^{T58A}, and MYC^{V394D} all significantly decreased reporter activation upon treatment with the STING agonist MSA2 (Figs. 3, E and F, and S1, E and F). Moreover, the inhibition of STING signaling by these three MYC variants was dependent on gene dosage, with higher MYC expression levels leading to increased suppression of the ISRE reporter (Fig. 2E). In contrast, overexpression of MYC^{L420P} allowed full activation of the reporter, independently of expression levels (Figs. 2E, S1, C and D). Taken together, these results show that DNA-binding activity of MYC is essential for the regulation of STING expression and downstream signaling, whereas STING regulation by MYC is independent of MIZ1.

No evidence of direct suppression of the STING promoter by MYC

Because of the observed requirement of DNA-binding activity of MYC for STING suppression, we tested if MYC directly interacted with the STING promoter. We did not find evidence for the direct binding of MYC to the STING promoter using chromatin immunoprecipitation (ChIP-qPCR), whereas we did observe MYC binding to the previously reported MYC target gene *APEX1* (Fig. S1G). These data align with previously reported ChIP-Seq analyses in which STING was not identified as a direct MYC target (44), but are in contrast with a previously reported interaction of MYC with STING in taxol-resistant cells. These results did not provide evidence of MYC binding to STING, pointing to indirect regulation of STING expression by MYC. We additionally investigated whether MYC could regulate the STING promoter through DNA methylation, as previous studies have suggested a potential role for epigenetic regulation by MYC, including through the DNA methyltransferase DNMT1

MYC suppresses STING expression

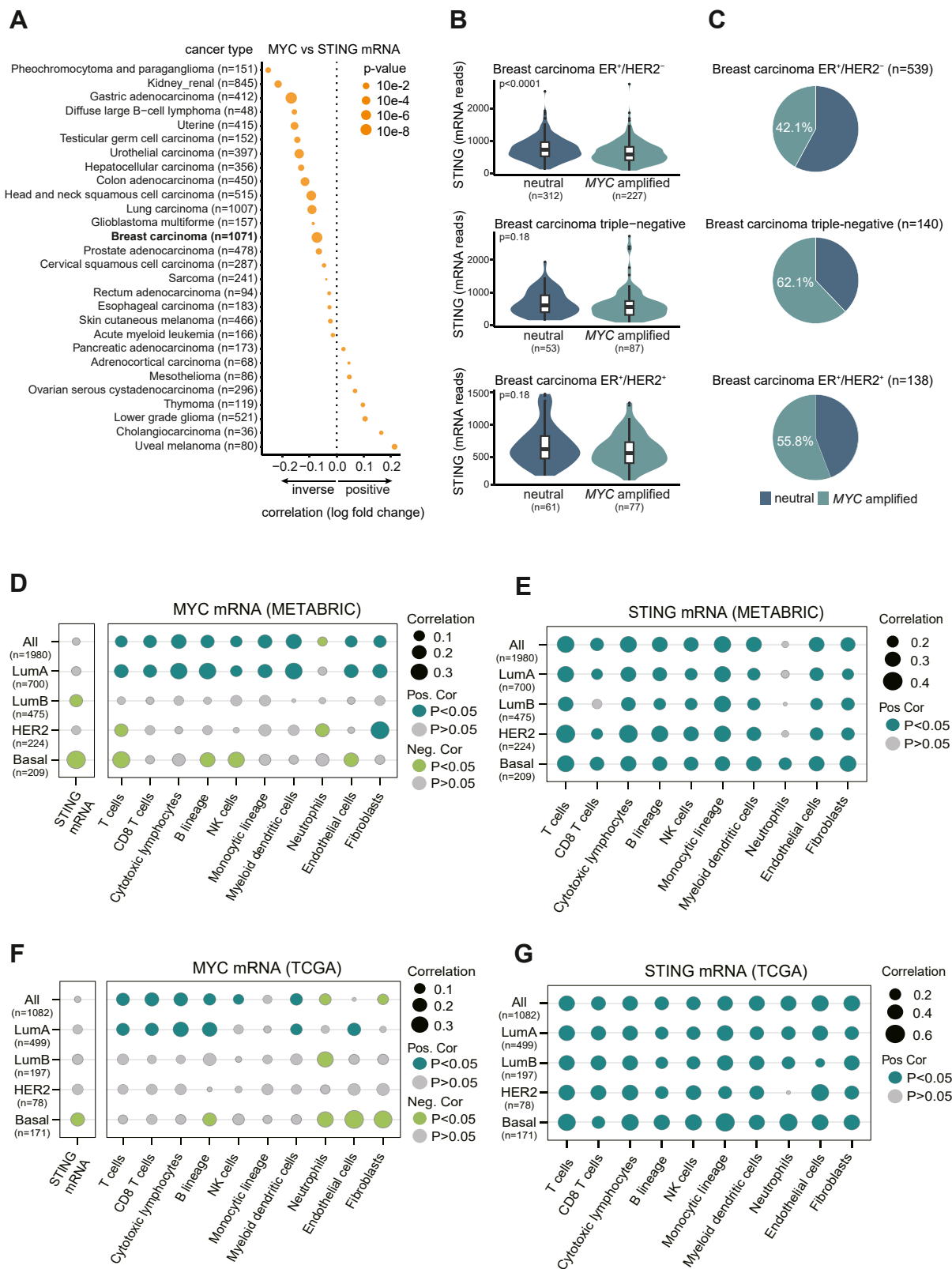


Figure 2. MYC mRNA expression is inversely correlated with STING mRNA and with immune cell composition. A, TCGA dataset analysis showing the correlation between MYC copy number and STING mRNA levels across various cancer types. B, separate analysis of different breast cancer subtypes within the "Breast carcinoma" group of TCGA, with indicated numbers of samples per subgroup. *p* values were calculated using the Mann–Whitney U test. C, the percentage of samples with MYC amplification per subgroup are indicated. D, correlation analysis between MYC mRNA expression and STING mRNA expression and immune cell composition in the METABRIC cohort. E, correlation analysis between STING mRNA expression and immune cell composition in the METABRIC cohort. F, correlation analysis between MYC mRNA expression and STING mRNA expression and immune cell composition in the TCGA breast cancer cohort. G, correlation analysis between STING mRNA expression and immune cell composition in the TCGA breast cancer cohort.

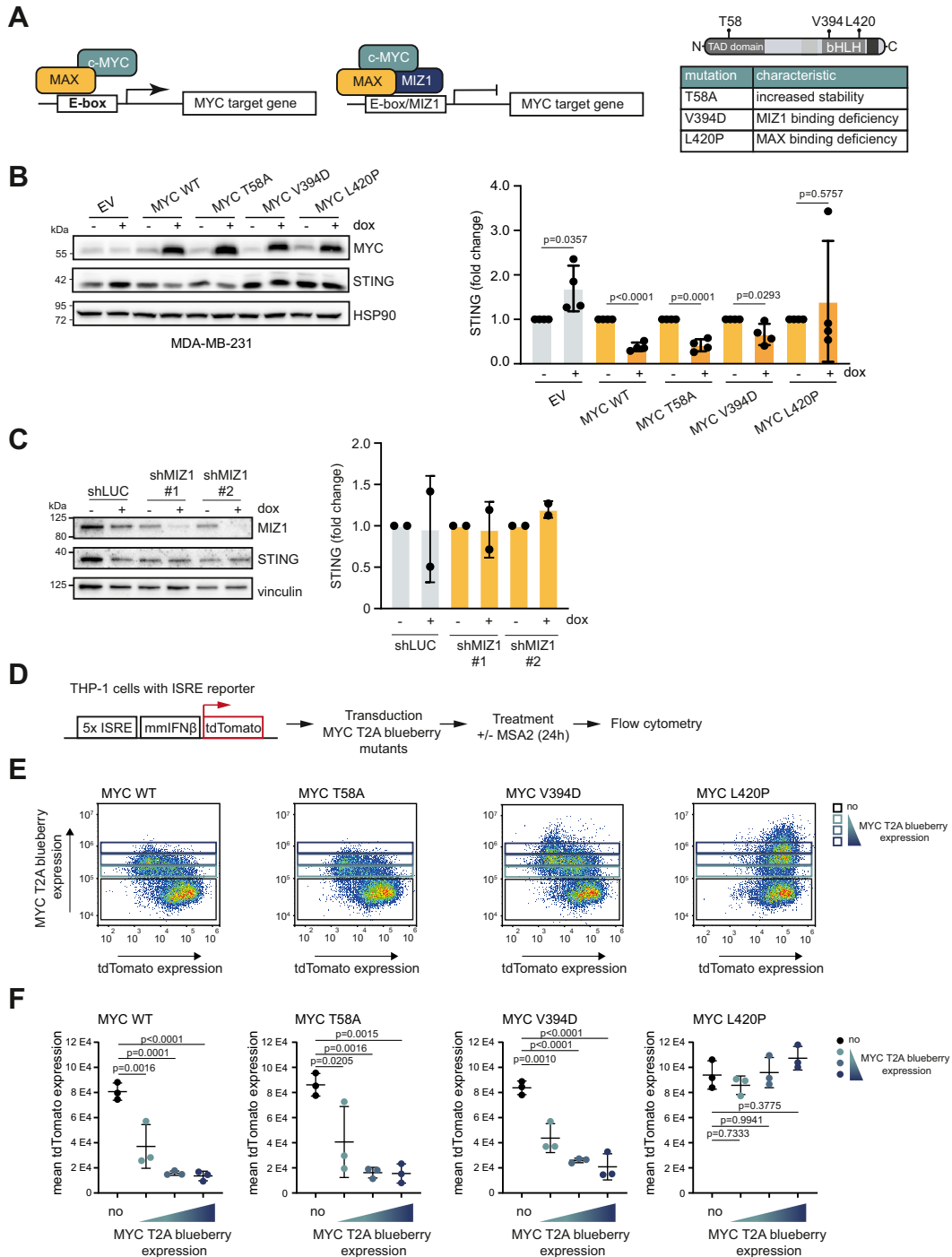


Figure 3. Regulation of STING by MYC requires its DNA-binding domain but is independent of MIZ1 binding. *A*, schematic overview of MYC variants with separation-of-function mutations affecting transcriptional activation and repression. *B*, immunoblotting for MYC, STING, and HSP90 in MDA-MB-231 cells expressing doxycycline (dox)-inducible MYC variants. Cells were treated with doxycycline for 72 h. Quantification of STING levels from four independent experiments. *p* values were calculated using a unpaired two-tailed Student's *t* test. *C*, immunoblotting for MIZ1, STING, and vinculin in BT-549 harboring the indicated shRNAs targeting MIZ1. Cells were treated with doxycycline for 72 h. *D*, graphical representation of the ISRE-driven tdTomato fluorescence reporter in THP-1 cells and the experimental treatment regimen for (*E*). *E* and *F*, ISRE-tdTomato reporter activity in THP-1 cells transduced with indicated MYC variants after treatment with MSA2 (10 μ M, 24 h). Representative flow cytometry plots are indicated in (*E*). Quantification of three biologically independent experiments is shown in (*F*). Means are indicated with and error bars that represent SD. *p* values were calculated using one-way ANOVA followed by Sidak's multiple comparisons test.

(45, 46). However, depletion of DNMT1 using siRNA did not prevent suppression of STING by MYC (Fig. S2A). To directly analyze the methylation status of the *STING* promoter, we used methylation-specific PCR. We did not observe altered

DNA methylation states of the *STING* promoter upon over-expression of MYC at multiple CpG sites (Fig. S2B). Combined, these data do not support a role for MYC in suppression of STING expression at the promoter level of the *STING* gene.

MYC suppresses STING expression

STAT1 and STAT3 control steady-state STING expression levels, and STAT3 cooperates in MYC-mediated STING regulation

STING expression is controlled by a positive feedback loop; STING activation leads to IFN signaling, while it is also an IFN-stimulated gene, which involves signaling *via* STAT1 (47). In agreement with such a regulatory network, MYC overexpression also resulted in the downregulation of protein levels of STAT1 (Fig. 1A). To explore a role of STAT1 signaling in the MYC-mediated suppression of STING, IFN-neutralizing antibodies were used to interfere with STAT1 activation. In line with expectations, IFN-neutralizing antibodies effectively prevented phosphorylation of STAT1 (Fig. 4A). Notably, despite the slight decrease in baseline STING protein levels, MYC-dependent regulation of STING still occurred in the absence of type I IFN signaling (Fig. 4A). Moreover, *STAT1* gene inactivation using CRISPR/Cas9 also did not prevent the upregulation of STING upon MYC depletion (Fig. 4B). Conversely, addition of recombinant IFN- β to the culture medium led to a slight increase in STING expression but did not prevent MYC-mediated downregulation of STING (Fig. 4C). Combined, these results show that a type I IFN feedback loop controls basal STING expression and additionally show that MYC operates independently of this feed-forward mechanism in regulating STING levels. In addition to STAT1, also STAT3 has been demonstrated to modulate inflammatory responses. In contrast to STAT1, STAT3 was shown to mediate protumorigenic effects and has been demonstrated to suppress STAT1-mediated antitumor immune responses (48, 49). To investigate the potential cooperative role of STAT3 and MYC in the regulation of STING, we generated *STAT3* KO BT-549 cells. In contrast to our expectations, and surprisingly similar to our findings in *STAT1* KO cells, basal STING expression levels were reduced in *STAT3* KO cells (Fig. 4D), indicating that both STAT1 and STAT3 are involved in driving basal levels of STING expression. In contrast to *STAT1* KO cells, *STAT3* KO cells did not show upregulation of STING upon MYC depletion, indicating that MYC cooperates with STAT3 in regulating STING levels (Fig. 4D). In line with these findings, depletion of STAT3 in *STAT1* KO cells resulted in an inability of MYC depletion to upregulate STING (Fig. 4E), which was observed in *STAT1* KO cells (Fig. 4B). To further investigate the role of STAT3 activation in the regulation of STING levels, *STAT3* KO cells were reconstituted with WT *STAT3* or a *STAT3* mutant that cannot be phosphorylated at tyrosine 705 (*STAT3*^{Y705F}) and does not respond to JAK signaling (Fig. 4F) (50). Whereas the low STING levels in *STAT3* KO cells were rescued upon reconstitution with WT *STAT3*, reconstitution with *STAT3*^{Y705F} failed to rescue STING levels. Together, these results show that basal STING expression levels are controlled by both STAT1 and STAT3 signaling and that STING expression can be modified by MYC in cooperation with STAT3.

MYC-mediated suppression of STING inhibits downstream activation of STAT1

Since STAT1 levels were found to be decreased upon MYC overexpression, we analyzed if the effects of MYC on STAT1

expression still occurred in *STING* KO cells. To this end, we downregulated MYC in *STING* KO BT-549 cells. Interestingly, and in contrast to the effects in *STING* WT cells, an increase in STAT1 expression following MYC depletion was not detected in *STING* KO cells (Fig. 4G). Conversely, re-expression of *STING* in *STING* KO cells resulted in enhanced STAT1 expression, thereby confirming the role of *STING* in the regulation of STAT1 (Fig. 4H). Moreover, not only the increase in STAT1 expression but also the increased CCL5 protein secretion upon MYC depletion was absent in *STING* KO cells (Fig. 4I). Importantly, stable expression of a *STING* complementary DNA (cDNA) driven by a constitutive promoter in cells overexpressing MYC successfully restored MYC-mediated downregulation of the chemokine CXCL10, further supporting the role of *STING* in MYC-mediated immune suppression (Fig. S3, B and C). Interestingly, whereas the modulation of MYC clearly impacted the protein levels of STAT1, MYC did not affect protein levels of STAT3 (Fig. 4, B and D). Combined, these findings indicate that MYC-mediated suppression of *STING* specifically impacts the activation of the type I IFN response downstream of *STING* and affects the balance between STAT1 and STAT3 signaling (Fig. 4J).

MYC suppresses irradiation or etoposide-induced chemokine production

To investigate whether MYC could inhibit immune responses induced by clinically used genotoxic anticancer treatments, BT-549 cells were treated with irradiation or with the topoisomerase inhibitor etoposide. Both irradiation and etoposide treatment induced the formation of micronuclei, of which a large fraction was cGAS-positive (Fig. 5, A and B). Both irradiation and etoposide treatment induced the expression of the IFN-stimulated genes CCL5 and ISG15, although the observed effects were modest (Fig. 5, C and D). Furthermore, no significant phosphorylation of STAT1 was observed, indicating that the activation of the type I IFN response was moderate (Fig. 5, C and D). Nevertheless, and in line with previous observations, production of these ISGs was effectively suppressed by the overexpression of MYC^{WT}, but not by MYC^{L420P} (Fig. 5, E and F). Moreover, both CCL5 and ISG15 induction upon etoposide depended on the expression of *STING*, since induction of CCL5 and ISG15 was virtually absent in *STING* KO cells (Fig. 5D). Together, these data show that MYC can effectively dampen chemokine production induced upon either irradiation or etoposide treatment.

MYC suppresses migration and activation of immune cells

Consistent with previous findings (20), we observed that MYC depletion caused upregulation of chemokines involved in mediating immune cells migration to tumor cells (Fig. 6A). To investigate whether MYC could also modulate the etoposide-induced attraction of peripheral blood mononuclear cells (PBMCs), we measured migration of PBMCs towards tumor cells in transwell assays (Fig. 6B). Etoposide led to an increase of approximately 30% in immune cell migration to BT-549 cells (Fig. 6C). Importantly, MYC

MYC suppresses STING expression

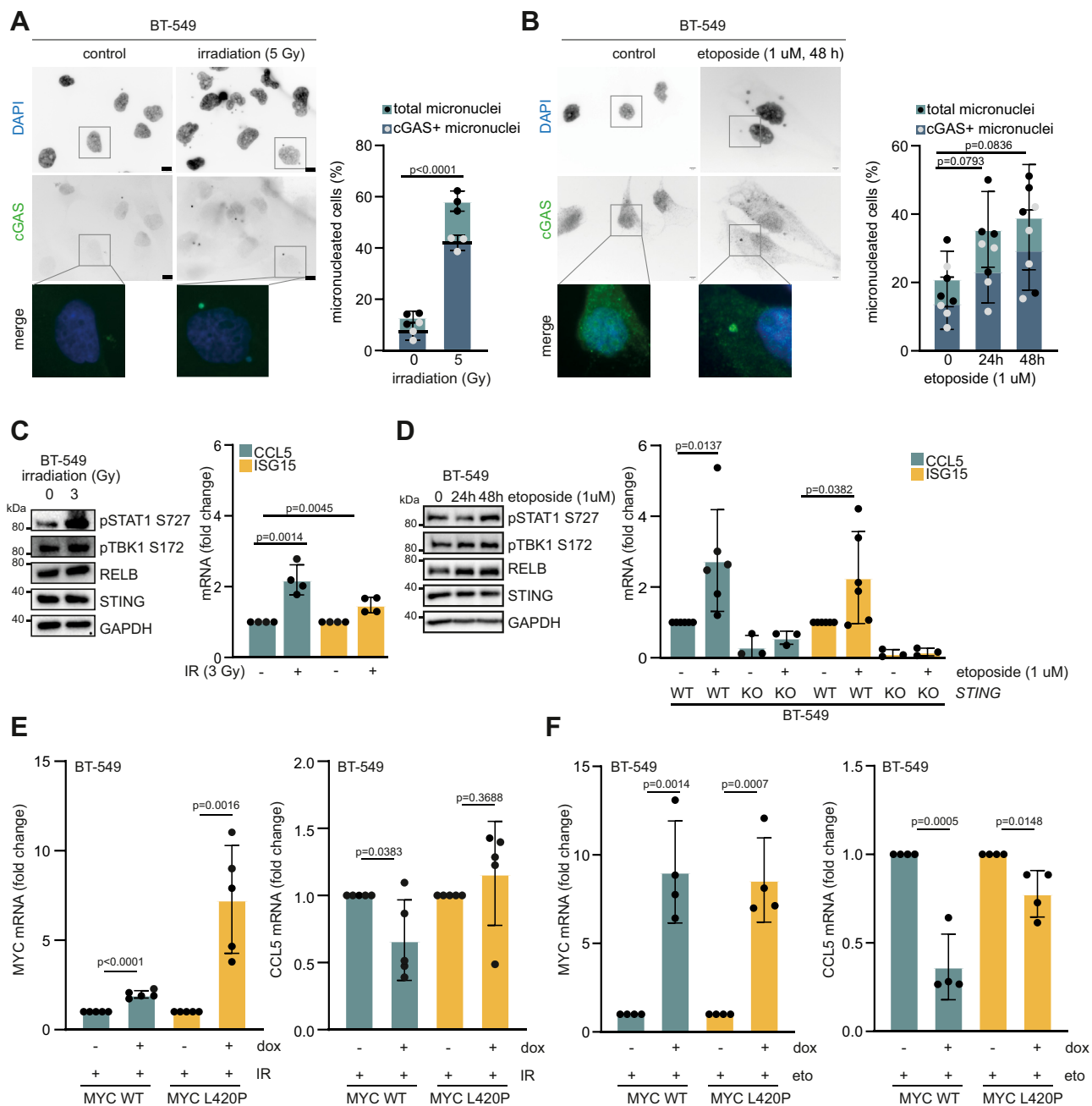


Figure 5. MYC suppresses irradiation or etoposide-induced chemokine production. *A*, representative immunofluorescence images of BT-549 cells, either left untreated (control) or irradiated (5 Gy), stained with DAPI (blue) and anti-cGAS (green). Scale bar represents 10 μ M. Quantification of cGAS-positive micronuclei is shown, with error bars representing the SD of three independent experiments. *B*, representative immunofluorescence images of BT-549 cells, either left untreated (control) or treated with etoposide (1 μ M) BT-549 for 48 h; cells at different time points. Scale bar represents 5 μ M. Quantification of cGAS-positive micronuclei is indicated for multiple treatment periods, with error bars representing the SD of three independent experiments. *C*, BT-549 cells were irradiated (3 Gy) and immunoblotted for pSTAT1, pTBK1, RELB, and STING, and qPCR analysis was done for CCL5 and ISG15 expression. Error bars represent the SD of four independent replicates. *D*, BT-549 *STING* WT and *STING* KO cells were treated with etoposide (3 Gy) and immunoblotted for pSTAT1, pTBK1, RELB, and STING, and qPCR analysis was done for CCL5 and ISG15 expression. Data of at least three independent replicates are plotted. *E* and *F*, qPCR analysis of MYC and CCL5 expression in MYC WT (blue) and MYC L420P (yellow) overexpressing cells after irradiation (IR) ($n = 5$, panel *E*) or etoposide (eto) treatment ($n = 4$, panel *F*). Throughout the figure, statistical analysis was done using unpaired two-tailed Student's *t*-tests.

Immunoblotting was performed for MYC, STAT1, STAT3, STING, and actin of one biological replicate. *G*, BT-549 *STING* WT and KO cells with indicated shRNAs were treated with doxycycline for 72 h. Immunoblotting was performed for MYC, STAT1, STING, and vinculin of one biological replicate. *H*, BT-549 *STING* KO cells were transduced with *STING* cDNA. Immunoblotting was performed for MYC, STAT1, STAT3, and actin of one biological replicate. *I*, quantification of CCL5 protein production in BT-549 cells with shMYC, assessed by ELISA after dox treatment for 72 h. Means and SD of six biologically independent experiments is plotted. *J*, schematic representation of the roles of MYC, STAT1, and STAT3 in controlling STING levels. Statistical analysis in this figure was done using an unpaired two-tailed Student's *t* test.

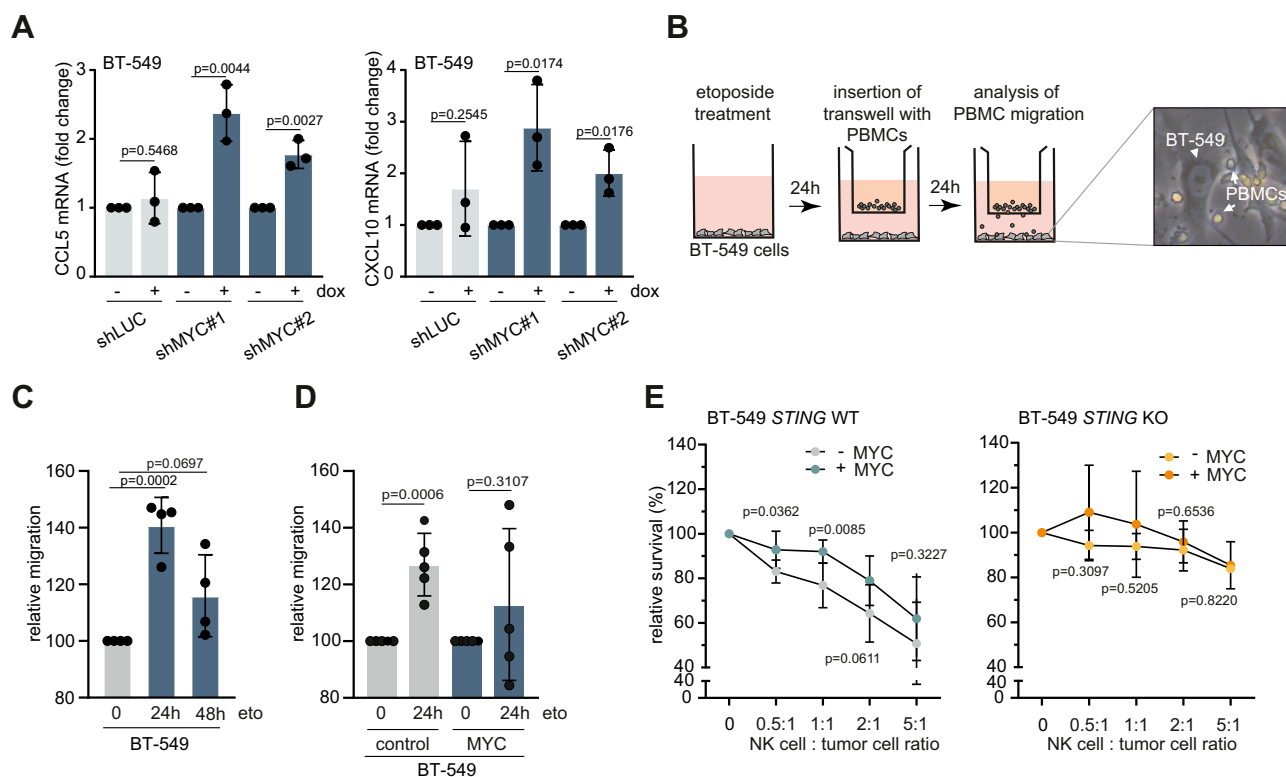


Figure 6. MYC inhibits immune cell migration and activation. *A*, qPCR analysis of CCL5 and CXCL10 expression following MYC depletion using indicated shRNAs in BT-549 cells. Means and SD of three independent experiments is shown. Statistical analysis was done using an unpaired two-tailed Student's *t* test. *B*, schematic representation of transwell assays with a brightfield image showing BT-549 cells (arrowhead) and PBMCs (arrows). *C* and *D*, quantification of PBMC migration in transwell assays represented in (*B*) with BT-549 cells with doxycycline-inducible MYC overexpression, based on four and five independent experiments, respectively. *p* values were calculated using an unpaired two-tailed Student's *t* test. *E*, analysis of NK cell-mediated killing of BT-549 *STING* WT cells ($n = 6$ independent experiments) and BT-549 *STING* KO cells ($n = 3$ independent experiments). BT-549 cells harbored doxycycline-inducible MYC overexpression and were plated at indicated ratios with NK cells. Statistical analysis was performed using a two-tailed Student's *t* test for each ratio, with error bars representing the SD.

overexpression led to a decrease in PBMC migration (Fig. 6D). To explore whether tumor cell-intrinsic MYC expression was also to reduce immune cell-mediated killing, we measured the ability of NK cells to kill tumor cells. To this end, we used the NK-92 cell line, displaying the characteristics of activated NK cells, to perform NK cytotoxicity assays (51). MYC overexpression in tumor cells prevented NK cell-mediated tumor cell killing, when compared to non-MYC-overexpressing tumor cells (Fig. 6E). Furthermore, tumor cell killing was nearly absent in *STING* KO cells (Fig. 6E), suggesting that *STING* plays a critical role in NK cell-mediated killing of MYC-overexpressing tumor cells. Together, these results imply that MYC overexpression in these tumor samples are impacting the tumor microenvironment.

Discussion

STING has been reported to play a major role in the activation of an inflammatory response upon chemotherapy and radiotherapy (12, 15, 17, 52). In line with this notion, *STING* expression and the activation of a type I IFN response were reported to have predictive value for therapy response in patients with TNBC (12, 53). *STING* is differentially expressed across cancer types, with variation in expression being explained by both genetic and epigenetic alterations (54). In this work, we

revealed that MYC and *STING* expression show an inverse correlation across cancer types and that MYC represses *STING* expression.

The interaction between *STING* and its downstream pathway components was reported to mainly occur at perinuclear *STING* foci (55, 56). Interestingly, previous reports have demonstrated that high levels of MYC were associated with decreased formation of perinuclear *STING* foci in TNBC (11, 57). Also, MYC was shown to dampen the effectiveness of pharmacological activation of *STING* by vadimezan (20). In line with these studies, we noted a decrease in *STING* signaling in MYC-overexpressing cells stimulated with the *STING* agonist MSA2. This observed limited activation and functionality of the *STING* signaling pathway could be explained by our observation that MYC suppresses *STING* mRNA and protein levels. In fact, we found that MYC-mediated downregulation of *STING* affects downstream factors of the inflammatory response such as *STAT1* expression and *STAT1* target proteins, including CCL5, CXCL10, and ISG-15. These observations align well with earlier reports, demonstrating that interference with MYC significantly enhanced cytokine production in a *STING*-dependent manner (46). Together, these results suggest that MYC-mediated suppression of *STING* plays an important role in the repression of downstream proteins that are part of the type I IFN-positive feedback loop.

MYC suppresses STING expression

We found that the ability of MYC to interact with MAX, which facilitates DNA binding, is essential for the negative regulation of STING. We also found that binding of MYC to the transcriptional repressor MIZ1 is dispensable for suppressing STING expression. These observations are supported by our ChIP data, which did not show enhanced binding of MYC to the intragenic regions of *STING*, suggesting that MYC regulates STING through an indirect mechanism. However, this is in contrast with previous work that pointed towards a direct role of MYC in the suppression of genes that are part of the type I IFN response (20, 32, 46). This may reflect context-dependence of how MYC operates, although some studies have reported an indirect role of MYC in regulating the IFN response. For instance, MYC-mediated suppression of the type I IFN response was suggested to involve regulation of genes involved in vesicle transport (58, 59). In addition, it was previously shown that MYC regulates STING levels *via* modulation of DNMT1 (45), although we could not confirm such a regulatory role, and did not observe differences in the levels of *STING* promoter methylation. Strikingly, suppression of inflammatory signaling by MYC was recently demonstrated to depend on the regulation of factors upstream in the type-I IFN pathway (58). Specifically, deletion of *TBK1* was demonstrated to bypass a requirement for MYC expression in immune suppression (58, 59). The notion that STING activates TBK1 (48), and that TBK1 levels are not affected by MYC overexpression, highlight the potential relevance of MYC-mediated regulation of STING in immune suppression.

Interestingly, a recent study showed that MYC and STAT3 can simultaneously bind enhancers of genes in ER⁺ breast cancers and TNBCs (25). Moreover, STAT3 has been reported to be a positive regulator of MYC expression and combined expression of STAT3 and MYC is associated with tumor-promoting effects (60). In contrast, STAT1 was reported to be a negative regulator of MYC (61). We found that both STAT1 and STAT3 signaling are required to maintain steady-state expression levels of STING. However, whereas STAT1 is dispensable for STING regulation by MYC, we observed that MYC and STAT3 cooperate in regulating STING levels. Of note and expectedly, we observed that *STAT3* inactivation induced a stronger effect in preventing MYC-mediated STING regulation when compared to STAT3 siRNA. Given that MYC-mediated repression of STING affected STAT1 levels, but did not affect STAT3 levels, MYC might drive a more protumorigenic, STAT3-driven tumor microenvironment. A model in which MYC collaborates with other transcription factors in a context-dependent fashion might also explain both protumor and antitumor effects of type I IFN signaling, since STING signaling was associated with both the suppression of outgrowth of dormant metastasis (62) and a protumorigenic immunosuppressive tumor microenvironment (63, 64). Clearly, the transcriptional activity of MYC is required for the regulation of genes part of the type I IFN response. However, this regulation might be context- and tumor subtype-dependent and we showed that this may occur through

indirect mechanisms, involving the targeting of upstream regulators of inflammation such as STING, rather than inhibition of the entire type I IFN pathway.

Many clinically used therapeutic modalities, including chemotherapy and irradiation, induce DNA damage, thereby instigating inflammatory signaling. We show that both etoposide and irradiation induce a significant increase in micronuclei numbers. However, the downstream activation of inflammatory responses showed significant variability and was accompanied by only a moderate induction of inflammatory cytokines, with etoposide inducing higher levels of inflammatory signaling when compared to irradiation at the used dosages. These findings suggest that the initiation of these responses is not exclusively reliant on micronuclei formation and cGAS activity. This observation is in line with recent studies, which show that micronuclei *per se* have limited capacity in the activation of the cGAS (65–67). In fact, cGAS is normally located in the nucleus, and organization of DNA in nucleosomes limits its auto-activation (68). In contrast to the ability of micronuclei to induce cGAS activity, cGAS-positive chromatin bridges were associated with a strong induction of interferon response (69). Although the role of cGAS-positive micronuclei is currently under debate, STING is documented to function as a central signaling hub, integrating inputs from multiple DNA sensors, also beyond cGAS (70). Of note, we observed that etoposide-induced chemokine production was dependent on STING. Whether chemokine induction in this setting was cGAS-dependent remains to be tested. Together, these observations underscore the pivotal role of STING signaling in response to diverse treatment modalities and diverse sources of DNA damage. Therefore, MYC-mediated suppression of STING might not only explain the inhibition of the type I IFN response upon irradiation and etoposide treatment but might also be relevant for inflammatory signaling in response to other genotoxic agents. Moreover, these findings may explain reduced attraction and activity of immune cells in the tumor microenvironment.

Taken together, MYC has a clear role in the tumor cell-intrinsic suppression of inflammatory responses that are induced upon genotoxic insults, which results in decreased immune cell migration and activity. Given the clear inverse correlation between MYC and STING across various cancer types, and the critical role of STING in IFN signaling, MYC could serve as a significant biomarker for predicting the effectiveness of immune-targeted therapies. Furthermore, therapeutic interference with MYC function may represent a promising strategy to boost immune checkpoint inhibitor treatment of MYC-overexpressing cancers.

Experimental procedures

Public data analysis

TCGA data acquisition

From TCGA, we extracted the preprocessed and normalized level of 3 RNA-seq (version 2) data for different cancer datasets available at the Broad GDAC Firehose portal (downloaded

January 2017 <https://gdac.broadinstitute.org/>) (35). For each sample, we downloaded RNA-Seq with Expectation Maximization gene normalized data (identifier: illuminahisec_rna-seqv2- RSEM_genes_normalized). RNA-Seq expression level read counts were normalized using FPKMUQ (Fragments per Kilo-base of transcript per Million mapped reads upper quartile normalization). This dataset is referred to as the TCGA-dataset throughout this manuscript. In addition, we collected preprocessed segmented somatic CNA data for each of the cancer datasets (identifier: genome_wide_snp_6 segmented_scna_minus_germline_cnv_hg19), which was generated with the Affymetrix Genome-Wide Human SNP Array 6.0. In short, the copy number segmentation pipeline implemented by TCGA and applied to Affymetrix SNP Array 6.0 uses a fully open-source tool Birdsuite and the DNACopy R-package to perform a circular binary segmentation analysis. Circular binary segmentation translates noisy intensity measurements into chromosomal regions of equal copy number. The final output files are segmented into genomic regions with the estimated copy number for each region. Next, the copy number values are transformed into segment mean values, which are equal to $\log_2(\text{copy number}/2)$ https://docs.gdc.cancer.gov/Data/PDF/Data_UG.pdf, (71–73).

Classification of TCGA samples based on copy number data

For STING1 mRNA analysis, TCGA samples were categorized into two groups (*MYC* “amplified” and “neutral”). Samples with a $\log_2(\text{copy number}/2)$ value of *MYC* greater than 0.3 were categorized as “amplified” (A_{MYC}). Samples with a copy number variation value of *MYC* between -0.3 and 0.3 were categorized as “neutral” (N_{MYC}). Differential mRNA expression analysis was conducted between samples of class A_{MYC} and N_{MYC} using the following steps. Firstly, subsets of samples were considered for separate analysis based on tumor subtype. Secondly, median STING1 mRNA expression values for samples in class A_{MYC} were compared to the mean STING1 mRNA expression values for samples in class N_{MYC} using Mann-whitney U test. Lastly, a metric was obtained from the Mann-Whitney U test as $-\log_{10}(p\text{-value}) \cdot \text{sign}(\text{difference between median STING1 expression in the samples of class } A_{MYC} \text{ and } N_{MYC})$.

Immune cell composition analysis in TCGA and METABRIC data

For the estimation of immune cell composition, the R package Microenvironment Cell Populations-counter (MCP-counter) was used (74). MCP-counter is a transcriptome-based deconvolution method to estimate the abundance scores of immune cell populations from RNA-seq data. RNA-seq data and breast cancer molecular subtype annotations in the TCGA and Molecular Taxonomy of Breast Cancer International Consortium (METABRIC) breast cancer cohorts were obtained from the cBioPortal to perform the MCP-counter analysis (<https://www.cbioportal.org/>) (71, 72). For METABRIC, the gene name *STING1* was used for STING mRNA analysis. For TCGA, *TMEM173* was used for STING mRNA analysis.

Human cell lines

Human breast cancer cell lines BT-549, MDA-MB231, HCC-1806, and MCF7 were obtained from ATCC (CRL-2314, CRM-HTB-26, CRL-2335, HTB-22). Cell line identity was confirmed using STR profiling. BT-549 and HCC-1806 were cultured in Roswell Park Memorial Institute medium supplemented with 10% fetal calf serum (FCS; Gibco) and penicillin/streptomycin (Gibco; 100 units per mL). MDA-MB-231 and RPE-1 (CRL4000) cells were cultured in low glucose (1 g/L) Dulbecco’s Modified Eagle Medium (Gibco), MCF7 cells were cultured in high glucose (4.5 g/L) Dulbecco’s Modified Eagle Medium (Gibco), all supplemented with 10% FCS and penicillin/streptomycin (100 units per mL). Cell lines were cultured at 37 °C in a humidified incubator with 5% CO₂ and were regularly tested for *mycoplasma*. All cell lines containing Dox-inducible DNA constructs were cultured in tetracycline-free FCS (Takara Bio USA).

The THP-1 cell line, expressing a ISRE-driven tdTomato reporter, was a gift from R. Luteijn (Utrecht University) and was cultured in Roswell Park Memorial Institute medium supplemented with 10% FCS, penicillin/streptomycin (100 units per mL), and glutamine (2 mM) (42). The NK-92 cell line (CRL-2407, ATCC) was cultured in Alpha-MEM with (deoxy) ribonucleosides supplemented with 12.5% horse serum, 10% FCS, and 1% penicillin/streptomycin. Every 72 h, IL-2 was added to NK-92 cells to a final concentration of 1000 U/ml.

Generation of cell lines

BT-549 and MDA-MB-231 cells were transduced with lentiviral tet-pLKO puro plasmids, encoding shRNAs. Tet-pLKO-puro was a gift from Dmitri Wiederschain (Addgene plasmid #21915). shRNA sequences that were used are as follows: *MYC*#1 (5'-CCC-AAG-GTA-GTT-ACT-CTT-AAA-3'), *MYC*#2 (5'-CAG-TTG-AAA-CAC-AAA-CTT-GAA-3') (73), luciferase (“shLUC”, 5'-AAG-AGC-TGT-TTC-TGA-GGA-GCC-3'), MIZ1#1, (5'-TGT-CCA-AGC-ACA-TCA-TCA-TTC-3'), and MIZ1#2 (5'-GTG-TTC-ACT-TTA-AGG-CTC-ATA-3'). Transduced cells were selected in medium containing puromycin (1 ug/ml). To generate MYC-overexpressing cell lines, BT-549 cell lines were transduced with pRRL-SFFV-IRES-mBlueberry, containing variants of MYC that were generated with mutagenesis PCR or synthesized as gene blocks (Genscript). To generate cell lines with dox-inducible MYC overexpressing constructs, BT-549 cell lines were transduced with pRetroX-Tet-On Advanced (Clontech). Subsequently, BT-549 cells harboring pRetroX-Tet-On Advanced were transduced with pRetroX-Tight-Pur containing MYC as described earlier (75). Additionally, MYC variants were cloned into pCW-puro, a gift from Alessia Ciarrocchi and Gloria Manzotti (Addgene plasmid # 184708), to create Dox-inducible overexpression of MYC variants. Moreover, MCF7 cells were transduced with pCW-puro EV and pCW-puro MYC-WT to establish Dox-inducible MYC overexpression in MCF7 cells.

For transduction, lentiviral particles were produced using HEK-293T cells (ATCC; CRL3216), which were transfected

MYC suppresses STING expression

with 5 µg lentiviral construct, in combination with packaging plasmids pMD2.G (Addgene plasmid #12259) and psPAX2 (Addgene plasmid #12260), both gifts from Didier Trono. Virus-containing supernatant was harvested at 48 and 72 h after transfection and filtered through a 0.45 µm syringe filter and used to infect target cells in one or two consecutive 24 h periods.

For the generation of *STAT1*, *STAT3*, and *STING* KO cell lines, CRISPR-Cas9 was used. *STAT1* and *STAT3* were edited using the sSpCas9(BB)-2A-Puro V2.0 (PX549, a gift from Feng Zhang (Addgene plasmid, 62,988)) plasmid as described elsewhere (64). The following guides were used: *STAT1*: 3'-TCCGCAACTATAGTGAACCT-5', *STAT3*: 3'-GGCCATCCTGCTAAAATCAG-5'. BT-549 cells were transfected with 2 µg of the indicated plasmid using FuGene (Promega Corporation), according to manufacturer's protocol. Forty eight hours after transfection, cells were selected with puromycin (1 µg/ml; Invivogen) for 48 h. Subsequently, cells were single cell sorted using a Sony flow cytometer (SH800s). Individual clones were validated by immunoblotting. pLentiCRISPRv2-STING-gRNA3 (targeting sequence 3'-AGGTACCGGAGAGTGTGCTC-5') was a gift from Nicolas Manel (Addgene plasmid #127640) (76) and was used to create *STING* KO cells using lentiviral transduction as described above.

siRNA transfection

siRNA transfection was performed using oligofectamine (Invitrogen) according to manufacturer's protocol with the following sequences: siSTAT3#1: 5'(GCA-GCA-GCU-GAA-CAA-CAU-G)TT 3' (77), siSTAT3#2: 5'(AAC-AUC-UGC-CUA-GAU-CGG-CUA)-TT 3' (78), siDNMT#1: 5'(UGU-AAC-UCU-ACG-UCU-CUU-C)TT 3', and siDNMT#2: 5'(GGA-ACU-UUG-UCU-CCU-UCA-A)TT 3'. As a control, siRNA duplex negative control (siSCR, Eurogentec) was used. BT-549 cells were treated with Dox (1 µg/ml) for 48 h prior to siRNA treatment.

Mutagenesis PCR

To create cell lines with MYC variant overexpression in a background in which endogenous MYC was depleted using shMYC#2, mutagenesis PCR was performed on pRRL-SFFV-IRESmBlueberry plasmids harboring MYC to introduce silent mutations that make MYC resistant to shMYC#2. To this end, the following codons were altered to create silent mutations in the shRNA-targeting region (K430 AAA → K430 AAG; L431 CTT → L431 CTG; H429 CAC → H429 CAT). Mutations were created by performing PCR in three consecutive steps using the following oligos respectively: MYC_H429H_forward: 5'AACGACGAGAACAGTTGAAACATAAACTTGAACAGCTACGGAAC3', MYC_L431L_forward: CGAGAACAGTTGAAACATAAACTTGAACAGCTACGGAAC3', MYC_K430K_forward: CGACGAGAACAGTTGAAACATAAAGCTGGAACAGCTACGGAAC3', and Phusion High Fidelity DNA polymerase (M0530S; New England Biolabs). PCR products were digested with DNP1, isolated using Qiaquick gel

extraction kit (Qiagen), and transformed into Stbl3 bacteria (Life Technologies).

Western blotting

Cells were lysed in Laemmli buffer (4% SDS, 20% glycerol, 125 mM Tris-HCl, pH 6.8) or Mammalian Protein Extraction Reagent (Thermo Scientific), supplemented with Halt protease inhibitor and Halt phosphatase inhibitor (Thermo Fisher Scientific; 1:100). Protein concentrations were measured using Pierce BCA Protein Assay Kit (Thermo Fisher Scientific). Proteins were separated by SDS-PAGE gel electrophoresis, transferred to polyvinylidene difluoride membranes (Merck Millipore), and blocked in 5% skimmed milk (Sigma-Aldrich) or 3% BSA in 0.05% TBS-Tween (Sigma-Aldrich). Immunodetection was performed with antibodies directed against β-actin (MP Biomedicals, 69,100, 1:1000), Vinculin (Abcam, ab129002, 1:1000), c-MYC (Abcam, ab32072, 1:1000), *STAT1* (Cell signaling, #9172, 1:1000), *STAT3* (Santa Cruz Biotechnology, sc482, 1:1000), *STING* (Cell signaling, #13647, 1:1000), cGAS (Cell signaling, #15102S, 1:1000), *TBK1* (Cell signaling, #3504, 1:1000), *IRF3* (Cell signaling, #4302, 1:1000), *PIRF3* (Cell Signaling, #29047, 1:1000), p*STAT1* S727 (Cell signaling, #8826, 1:1000), p*STAT1* Y701 (Cell signaling, #9167, 1:1000), p*NFκB* (Cell Signaling, #3033, 1:1000), *laminA/C* (Cell Signaling, #4777, 1:1000), and *MIZ1* (Santa Cruz, sc-136985, 1:1000), *Tubulin* (Abcam, ab44928, 1:5000), *HSP90* (Santa Cruz Biotechnology, sc-13119, 1:10,000), *DNMT1* (Abcam, ab188453, 1:1000), *GAPDH* (Abcam, ab128915, 1:10,000). Horseradish peroxidase (HRP)-conjugated secondary antibodies (DAKO, 1:10,000) were used for detection. Alternatively, anti-Actin-HRP (Proteintech, HRP-60008, 1:1000) was used. Visualization was done using chemiluminescence (LumiLight, Roche Diagnostics) on a Bio-Rad bioluminescence device, equipped with Quantity One/ChemiDoc XRS software (Bio-Rad). Quantification was conducted using Fiji, with the results normalized against the loading controls.

Quantitative reverse transcription-PCR

Cell pellets of BT-549 cells treated with or without dox (1 µg/ml) for indicated time points were harvested, snap frozen, and stored at -20 °C. RNA was isolated using the RNeasy Mini Kit (Qiagen) and cDNA was synthesized using the iScript cDNA synthesis kit (Biorad), according to the manufacturer's instructions. Quantitative reverse transcription-PCR for cytokine mRNA expression levels was performed in triplicate using PowerUp SYBR Green Master Mix (Thermo Fisher Scientific). β-Actin was used as a reference and experiments were performed on an Applied Biosystems Fast 7500 device. The following primer sequences were used: β-actin forward: 5'-ACT-CTT-CCA-GCC-TTC-CTT-CC-3', reverse: 5'-CAA-TGC-CAG-GGT-ACA-TGG-TG-3' (Invitrogen), *CCL5* forward: 5'-CCA-GCA-GTC-GTC-TTT-GTC-AC-3', reverse: 5'-CTC-TGG-GTT-GGC-ACA-CAC-TT-5' (Invitrogen), *ISG15* forward: 5'-TGG-ACA-AAT-GCG-ACG-AAC-CTC-3', reverse: 5'-TCA-GCC-GTA-CCT-CGT-AGG-TG-3' (Origene), c-MYC forward: 5'-TGA-GGA-GAC-ACC-GCC-

CAC-3', reverse: 5'-CAA-CAT-CGA-TTT-CTT-CCT-CA T-CTT-C-3' (Origene), CXCL10 forward: 5'-AGC-AGA-GGA-ACC-TCC-AGT-CT-3', reverse: 5'-AGG-TAC-TCC-TTG-AAT-GCC-ACT-5' (Invitrogen).

IFN neutralizing antibodies

For culture with type I IFN-neutralizing antibodies, BT-549 cells with indicated shRNAs were seeded in 6-well plates (100,000 cells/well) and treated with dox (1 µg/ml) and IFN neutralizing antibodies (1:500, PBL assay Science) for 5 days. Expression of indicated proteins was analyzed using Western blot.

Enzyme-linked immuno sorbent assay

To measure secretion of CCL5, BT-549 cells with indicated shRNAs were treated with or without dox (1 µg/ml) for 5 days and plated at similar cell densities in 6-well plates (50,000 cells/well). Culture media was harvested at indicated time points and stored at -20 °C. Concentrations of CCL5 (R&D Systems, DY278-05) were measured using ELISA according to manufacturer's instructions.

Immunofluorescence microscopy

Cells were grown on coverslips and treated with or without doxyc (1 µg/ml) for indicated time points and irradiated with indicated dose using a CIS international/IBL 637 cesium¹³⁷ source. After 72 h, cells were washed with PBS and fixed in 2% formaldehyde in PBS for 15 minutes at room temperature. Subsequently, cells were permeabilized with 0.1% Triton X-100 in PBS for 1 minute followed by blocking in 0.05% Tween-20 and 2.5% BSA in PBS for 1 h. Cells were incubated overnight with primary antibodies against cGAS (1:200, Cell Signaling, #15102) in PBS-Tween-BSA. Cells were extensively washed and incubated for 1 h with Alexa488-conjugated secondary antibodies (1:400, Invitrogen, A-11008) at room temperature, shielded from light. Subsequently, DAPI was added for 10 min (Sigma). Slides were mounted with ProLong Gold Antifade Mountant (Invitrogen, P36934). Images were acquired on a Leica DM-6000RXA fluorescence microscope, equipped with Leica Application Suite software, using a 63x magnification. Pictures were processed using Fiji software.

Flow cytometry

THP-1 cells were cultured and treated with MSA2 (5 µM, Axon Medchem) for 24 or 48 h. Subsequently, cells were collected, washed twice with PBS, and measured on a Novo-Cyte Quanteon (Aligent). Data was analyzed using NovoExpress software.

Chromatin immunoprecipitation-PCR

ChIP was essentially performed as described elsewhere (79, 80).

Briefly, BT-549 cells expressing pRetrox-EV or pRetrox-MYC were treated with Dox (10 ng/ml) for 72 h. ChIP was performed using c-MYC antibody (Abcam, ab32072). PCR was

performed using the following primer pairs: APEX1 (positive control), forward: 5'-GGC-GGG-ACC-TGG-TGC-GGG-GA-3', reverse: 5'-ACC-GCG-TCA-CCC-ACC-GAA-GCA-3' (81). For STING, three primer pairs were used and described before (46): #1 forward: 5'-ATC-CAG-CTT-GTA-GTA-AGT-GCT-CG-3', reverse: 5'-GCT-GTA-GTG-TCC-CTA-GCT-GGT-3', #2 forward: 5'-GCC-CAG-ATT-GTG-CCA-CTC-TA-3', reverse: 5'-CAG-GCT-GGT-CTT-GAA-TTC-TTG-A-3', #3 forward: 5'-TGA-CAC-ACC-CAG-AAT-AGC-ATC-C-3', reverse: 5'-GCC-CTT-CTC-TGA-GCT-GTA-GTG-3'.

Transwell migration assays

BT-549 cells with indicated constructs were plated in 6-well plates and pretreated with Dox (1 µg/ml) for 2 days followed by etoposide treatment (1µM) for 24 h. After this, cells were replated in 12-well plates (30,000 cells/well). Human PBMCs were isolated from peripheral blood from healthy volunteers (buffy coat obtained from Sanquin) by Ficoll-Paque density centrifugation (Ficoll-Paque PLUS, GE Healthcare Life Sciences). PBMCs (1,500,000/insert) were added on top of the filter membrane of a transwell insert (12-well cell culture insert, 3.0 µm pore PET translucent, cellQart) and incubated for 24 h, after which supernatant from the lower chamber was harvested to quantify migrated PBMCs by microscopy.

NK cytotoxicity assay

BT-549 cells with indicated constructs were pretreated with Dox for 3 days (1 µg/ml). Subsequently, BT-549 cells were seeded in 24-well plates (60,000 cells/well) and incubated overnight. The next day, BT-549 cells were washed with PBS. Then, NK-92 cells were added in the following effector to target ratios (NK-92:BT-549); 0:1, 1:2, 1:1, 2:1, and 5:1 and incubated for 4 h. Subsequently, NK-92 cells were removed, and cells were washed with PBS and stained with Coomassie Brilliant Blue solution, containing 50% methanol (Merck) and 14% acetic acid (Merck) for 20 min, and extensively washed with demineralized water. After plates were air-dried overnight, DMSO was added, and absorption values were measured at 595 nm using a Multiscan Sky microplate spectrophotometer (Thermo Fisher Scientific).

Methylation-specific PCR

Genomic DNA was purified from BT-549 cells treated with or without Dox (1 µg/ml) for 48 h. Subsequently, DNA was bisulfate converted using the EZ DNA methylation kit (Zymo Research). Primers to analyze the methylation status of multiple CpG sites within the STING (*TMEM173*) promoter were designed using the UCSC Genome Browser and MethPrimer (82). Bisulfite-treated DNA was amplified by PCR. All samples were loaded on 2% agarose gels, stained with Midori green, and visualized using a ChemiDoc (Bio-Rad). Leukocyte DNA and *in vitro* (IV) methylated DNA was used to validate the methylation-specific and unmethylation-specific primer sets. The following primer sets were used: β-actin forward: 5'-TAGGGAGTATATAGGTTGGGGAAAGTT-3', reverse: 5'-AACACACAATAACAAACACAAATTCAC-3',

MYC suppresses STING expression

JAM3 methylated forward: 5'- GGGATTATAAGTC GCGTCGC-3', reverse: 5'- CGAACGCAAACCGAAATCG-3'. JAM3 unmethylated forward: 5'-GTGGGGATTATAAG TTGTGTTGTG-3', reverse: 5'-CAACCAAACACAAAACCA AAATCAC-3', STING enhancer methylated forward: 5'- TTTGGGCGATAAGAGTAAAATTC-3', reverse: 5'- ATTCTTCTAACCTCTCTAAACGTA-3', STING enhancer unmethylated forward: 5'-TTGGGTGATAAGAGTAAAA TTTTGT-3', reverse: 5'-TTCTTCTAACCTCTCTAAACA TA-3', cg16983159 methylated forward: 5'- GGTTTTTT GTAGGAAATGGTTACGT-3', reverse: 5'- AACCTCAA- TAATCCACCCATCTCGAC-3', cg16983159 unmethylated forward: 5'- GGTTTTTTGTAGGAAATGGTTATGT-3', reverse: 5'-TAACCTCAAATAATCCACCCATCTCAAC-3', cg08321103 methylated forward: 5'-GTGATTTTTTTAAGA- GAGTTTGTCGGT-3', reverse: 5'- TCCCAAATAACT AAAATTACAAACG-3', cg22631913 methylated forward: 5'- GAGTTATTTGGAGTGGATGTGGCGT-3', reverse: 5'- ATCCCGTATCCCAAAAATCACGAA-3', cg22631913 unmethylated forward: 5'- TTGGGTGATAAGAGTAAAA TTTTGT- 3', reverse: 5'- ATTCTTCTAACCTCTCTAAA- CATA-3'.

Data analysis

Statistical testing was performed using the GraphPad Prism 8.4.2 (Dotmatics) and R version 4.4.0. All figure legends state the number of independent biological replicates and the statistical test used. The number of biological replicates for each Western blot images shown in the main manuscript is indicated in the figure legends. Western blots were quantified using ImageJ (version 1.53k) or Adobe Photoshop (Creative Cloud 2025) and corrected for the loading controls. No data was excluded from our study. The only exceptions were cases where the positive control of experiments did not work. In these instances, we deemed it necessary to exclude the data to maintain the integrity and validity of our results.

Data availability

TCGA data is downloaded from <https://gdac.broadinstitute.org/>. Source data are provided with this paper. The data analyzed in the current study are available from the corresponding author upon reasonable request.

Supporting information—This article contains supporting information.

Acknowledgments—We thank R. Luteijn (Utrecht University) for sharing the tdTomator reporter cell line. We thank X and Y for help with MSP analysis.

Author contributions—R. L. and M. A. T. M. v. V. writing—original draft; R. L. and C. S. visualization; R. L., C. S., F. J. B., M. E., A. B., S. D. v. B., and G. B. A. W. validation; R. L., F. J. B., M. E., A. B., B. v. D. V., and M. A. T. M. v. V. resources; R. L. and M. A. T. M. v. V. project administration; R. L., C. S., A. B., S. Y., G. B. A. W., R. S. N. F., and M. A. T. M. v. V. methodology; R. L., C. S., F. J. B., M. E., A. B., S. Y., S. D. v. B., and G. B. A. W. investigation; R. L., C. S., A. B., S.

Y., and G. B. A. W. formal analysis; R. L., C. S., F. J. B., A. B., S. Y., G. B. A. W., and M. A. T. M. v. V. data curation; R. L. and M. A. T. M. v. V. conceptualization; C. S., B. v. D. V., G. B. A. W., and M. A. T. M. v. V. writing—review and editing; A. B. and R. S. N. F. software; R. S. N. F., M. d. B., and M. A. T. M. v. V. supervision; M. A. T. M. v. V. funding acquisition.

Funding and additional information—This work has been funded by grants from the Dutch Cancer Society to M. A. T. M. v. V. (KWF-14516) and the Netherlands Organisation for Scientific Research to M. A. T. M. v. V. (NWO-VICI 09150182110019).

Conflict of interest—The authors declare that they have no conflicts of interests with the contents of this article.

Abbreviations—The abbreviations used are: cDNA, complementary DNA; cGAS, cyclic GMP-AMP synthase; ChIP, chromatin immunoprecipitation; Dox, doxycycline; FCS, fetal calf serum; HRP, horseradish peroxidase; IFN, interferon; ISRE, interferon-stimulated response element; MCP-counter, Microenvironment Cell Populations-counter; METABRIC, Molecular Taxonomy of Breast Cancer International Consortium; PBMC, peripheral blood mononuclear cell; STING, stimulator of interferon genes; TNBC, triple negative breast cancer.

References

1. Foulkes, W. D., Smith, I. E., and Reis-Filho, J. S. (2010) Triple-negative breast cancer. *N. Engl. J. Med.* **363**, 1938–1948
2. Lehmann, B. D., Colaprico, A., Silva, T. C., Chen, J., An, H., Ban, Y., *et al.* (2021) Multi-omics analysis identifies therapeutic vulnerabilities in triple-negative breast cancer subtypes. *Nat. Commun.* **12**, 1–18
3. Bareche, Y., Venet, D., Ignatiadis, M., Aftimos, P., Piccart, M., Rothe, F., *et al.* (2018) Unravelling triple-negative breast cancer molecular heterogeneity using an integrative multiomic analysis. *Ann. Oncol.* **29**, 895–902
4. Won, K.-A., and Spruck, C. (2020) Triple-negative breast cancer therapy: current and future perspectives (Review). *Int. J. Oncol.* **57**, 1245–1261
5. Kraya, A. A., Maxwell, K. N., Wubbenhorst, B., Wenz, B. M., Rech, A. J., Dorfman, L. M., *et al.* (2019) Genomic signatures predict the immunogenicity of BRCA- deficient breast cancer. *Clin. Cancer Res.* **25**, 4363–4374
6. Heijink, A. M., Talens, F., Jae, L. T., van Gijn, S. E., Fehrmann, R. S. N., Brummelkamp, T. R., *et al.* (2019) BRCA2 deficiency instigates cGAS-mediated inflammatory signaling and confers sensitivity to tumor necrosis factor- α -mediated cytotoxicity. *Nat. Commun.* **10**, 100
7. Voorwerk, L., Slagter, M., Horlings, H. M., Sikorska, K., Van De Vijver, K. K., De Maaker, M., *et al.* (2019) Immune induction strategies in metastatic triple-negative breast cancer to enhance the sensitivity to PD-1 blockade : the TONIC trial. *Nat. Med.* **25**, 920–928
8. Schmid, P., Cortes, J., Pusztai, L., McArthur, H., Kümmel, S., Bergh, J., *et al.* (2020) Pembrolizumab for early triple-negative breast cancer. *N. Engl. J. Med.* **382**, 810–821
9. Manguso, R. T., Pope, H. W., Zimmer, M. D., Brown, F. D., Juneja, V. R., Weiss, S. A., *et al.* (2017) In vivo CRISPR screening identifies Ptpn2 as cancer immunotherapy target. *Nature* **547**, 413–418
10. Patel, S. J., Sanjana, N. E., Kishton, R. J., Eidzadeh, A., Vodnala, S. K., Cam, M., *et al.* (2017) Identification of essential genes for cancer immunotherapy. *Nature* **548**, 537–542
11. Parkes, E. E., Humphries, M. P., Gilmore, E., Sidi, F. A., Bingham, V., Phyu, S. M., *et al.* (2021) The clinical and molecular significance associated with STING signaling in breast cancer. *NPJ Breast Cancer* **7**, 81
12. Parkes, E. E., Walker, S. M., Taggart, L. E., McCabe, N., Knight, L. A., Wilkinson, R., *et al.* (2017) Activation of STING-dependent innate immune signaling by s-phase-specific DNA damage in breast cancer. *J. Natl. Cancer Inst.* **109**, 1–10

13. Chen, J., Harding, S. M., Natesan, R., Tian, L., Benci, J. L., Li, W., *et al.* (2020) Cell cycle checkpoints cooperate to suppress DNA- and RNA-associated molecular pattern recognition and anti-tumor immune responses. *Cell Rep* **32**, 108080
14. Sun, L., Wu, J., Du, F., Chen, X., and Chen, Z. J. (2013) Cyclic GMP-AMP synthase is a cytosolic DNA sensor that activates the type-I interferon pathway. *Science* **339**, 786–791
15. MacKenzie, K. J., Carroll, P., Martin, C. A., Murina, O., Fluteau, A., Simpson, D. J., *et al.* (2017) CGAS surveillance of micronuclei links genome instability to innate immunity. *Nature* **548**, 461–465
16. Mackenzie, K. J., Carroll, P., Lettice, L., Tarnauskaitė, Ž., Reddy, K., Dix, F., *et al.* (2016) Ribonuclease H2 mutations induce a cGAS/STING-dependent innate immune response. *EMBO J* **35**, 831–844
17. Harding, S. M., Benci, J. L., Irianto, J., Discher, D. E., Minn, A. J., and Greenberg, R. A. (2017) Mitotic progression following DNA damage enables pattern recognition within micronuclei. *Nature* **548**, 466–470
18. Sporikova, Z., Koudelakova, V., Trojanec, R., and Hajdich, M. (2018) Genetic markers in triple-negative breast cancer. *Clin. Breast Cancer* **18**, e841–e850
19. Katsuta, E., Yan, L., Takeshita, T., McDonald, K., and Dasgupta, S. (2020) High MYC mRNA expression is more clinically relevant than MYC DNA amplification in triple-negative breast cancer. *Int. J. Mol. Sci.* **21**, 217
20. Zimmerli, D., Brambillasca, C. S., Talens, F., Bhin, J., Linstra, R., Romanens, L., *et al.* (2022) MYC promotes immune-suppression in triple-negative breast cancer via inhibition of interferon signaling. *Nat. Commun.* **13**, 6579
21. Annunziato, S., de Ruyter, J. R., Henneman, L., Brambillasca, C. S., Lutz, C., Vaillant, F., *et al.* (2019) Comparative oncogenomics identifies combinations of driver genes and drug targets in BRCA1-mutated breast cancer. *Nat. Commun.* **10**, 397
22. Tang, M., O'Grady, S., Crown, J., and Duffy, M. J. (2022) MYC as a therapeutic target for the treatment of triple-negative breast cancer: preclinical investigations with the novel MYC inhibitor, MYC1975. *Breast Cancer Res. Treat.* **195**, 105–115
23. Duffy, M. J., O'Grady, S., Tang, M., and Crown, J. (2021) MYC as a target for cancer treatment. *Cancer Treat. Rev.* **94**, 102154
24. Pelengaris, S., Khan, M., and Evan, G. (2002) c-MYC: more than just a matter of life and death. *Nat. Rev. Cancer* **2**, 764–776
25. Jakobsen, S. T., Jensen, R. A. M., Madsen, M. S., Ravnsborg, T., Vaagenso, C. S., Siersbæk, M. S., *et al.* (2024) MYC activity at enhancers drives prognostic transcriptional programs through an epigenetic switch. *Nat. Genet.* **56**, 663–674
26. Patange, S., Ball, D. A., Wan, Y., Karpova, T. S., Girvan, M., Levens, D., *et al.* (2022) MYC amplifies gene expression through global changes in transcription factor dynamics. *Cell Rep.* **38**, 1–17
27. Brenner, C., Deplus, R., Didelot, C., Loriot, A., Viré, E., De Smet, C., *et al.* (2005) Myc represses transcription through recruitment of DNA methyltransferase corepressor. *EMBO J* **24**, 336–346
28. Herold, S., Wanzel, M., Beuger, V., Frohme, C., Beul, D., Hillukkala, T., *et al.* (2002) Negative regulation of the mammalian UV response by Myc through association with Miz-1. *Mol. Cell* **10**, 509–521
29. Kress, T. R., Sabò, A., and Amati, B. (2015) MYC: connecting selective transcriptional control to global RNA production. *Nat. Rev. Cancer* **15**, 593–607
30. Dhanasekaran, R., Deutzmann, A., Mahauad-Fernandez, W. D., Hansen, A. S., Gouw, A. M., and Felsher, D. W. (2022) The MYC oncogene — the grand orchestrator of cancer growth and immune evasion. *Nat. Rev. Clin. Oncol.* **19**, 23–36
31. Kortlever, R. M., Sodik, N. M., Wilson, C. H., Littlewood, T. D., Evan, G. I., Kortlever, R. M., *et al.* (2017) Myc cooperates with ras by programming inflammation and immune suppression. *Cell* **171**, 1301–1315.e14
32. Muthalagu, N., Monteverde, T., Raffo-Iraolagoitia, X., Wiesheu, R., Whyte, D., Hedley, A., *et al.* (2020) Repression of the type I interferon pathway underlies MYC- and KRAS-dependent evasion of NK and B cells in pancreatic ductal adenocarcinoma. *Cancer Discov.* **10**, 872–887
33. Sodik, N. M., Kortlever, R. M., Barthet, V. J. A., Campos, T., Pellegrinet, L., Kupczak, S., *et al.* (2020) MYC instructs and maintains pancreatic adenocarcinoma phenotype. *Cancer Discov.* **10**, 588–607
34. Spranger, S., and Gajewski, T. F. (2018) Impact of oncogenic pathways on evasion of antitumor immune responses. *Nat. Rev. Cancer* **18**, 139–147
35. Ciriello, G., Miller, M. L., Aksoy, B. A., Senbabaoglu, Y., and Sander, C. (2013) Emerging landscape of oncogenic signatures across human cancers. *Nat. Genet.* **45**, 1127–1133
36. Curtis, C., Shah, S. P., Chin, S.-F., Turashvili, G., Rueda, O. M., Dunning, M. J., *et al.* (2012) The genomic and transcriptomic architecture of 2,000 breast tumours reveals novel subgroups. *Nature* **486**, 346–352
37. Sears, R., Nuckolls, F., Haura, E., Taya, Y., Tamai, K., and Nevins, J. R. (2000) Multiple Ras-dependent phosphorylation pathways regulate Myc protein stability. *Genes Dev.* **14**, 2501–2514
38. Welcker, M., Orian, A., Jin, J., Grim, J. A., Harper, J. W., Eisenman, R. N., *et al.* (2004) The Fbw7 tumor suppressor regulates glycogen synthase kinase 3 phosphorylation-dependent c-Myc protein degradation. *Proc. Natl. Acad. Sci. U. S. A.* **101**, 9085–9090
39. Wiese, K. E., Walz, S., Eyss, V., Wolf, E., Athineos, D., Sansom, O., *et al.* (2013) The role of MIZ-1 in MYC-dependent tumorigenesis. *Cold Spring Harb. Perspect. Med.* **3**, 1–10
40. Van Riggelen, J., Müller, J., Otto, T., Beuger, V., Yetil, A., Choi, P. S., *et al.* (2010) The interaction between Myc and Miz1 is required to antagonize TGFβ-dependent autocrine signaling during lymphoma formation and maintenance. *Genes Dev.* **24**, 1281–1294
41. Blackwood, E. M., and Eisenman, R. N. (1991) Max: a helix-loop-helix zipper protein that forms a sequence-specific DNA-binding complex with myc. *Science* **251**, 1211–1217
42. Luteijn, R. D., Zaver, S. A., Gowen, B. G., Wyman, S. K., Garelis, N. E., Onia, L., *et al.* (2019) SLC19A1 transports immunoreactive cyclic dinucleotides. *Nature* **573**, 434–438
43. Pan, B. S., Perera, S. A., Piesvaux, J. A., Presland, J. P., Schroeder, G. K., Cumming, J. N., *et al.* (2020) An orally available non-nucleotide STING agonist with antitumor activity. *Science* **369**, 935
44. Thomas, L. R., Adams, C. M., Wang, J., Weissmiller, A. M., Creighton, J., Lorey, S. L., *et al.* (2019) Interaction of the oncoprotein transcription factor MYC with its chromatin cofactor WDR5 is essential for tumor maintenance. *Proc. Natl. Acad. Sci. U. S. A.* **116**, 25260–25268
45. Wu, S. Y., Xiao, Y., Wei, J. L., Xu, X. E., Jin, X., Hu, X., *et al.* (2021) MYC suppresses STING-dependent innate immunity by transcriptionally upregulating DNMT1 in triple-negative breast cancer. *J. Immunother. Cancer* **9**, e002528
46. Lee, K., Lin, C.-C., Servetto, A., Bae, J., Kandagatla, V., Ye, D., *et al.* (2022) Epigenetic repression of STING by MYC promotes immune evasion and resistance to immune checkpoint inhibitors in triple negative breast cancer. *Cancer Immunol. Res.* **10**, 829–843
47. Ma, F., Li, B., Yu, Y., Iyer, S. S., Sun, M., and Cheng, G. (2015) Positive feedback regulation of type I interferon by the interferon-stimulated gene STING. *EMBO Rep.* **16**, 202–212
48. Chen, M., Linstra, R., and van Vugt, M. A. T. M. (2022) Genomic instability, inflammatory signaling and response to cancer immunotherapy. *Biochim. Biophys. Acta - Rev. Cancer.* **1877**, 188661
49. Liu, S., Liu, S., Yu, Z., Zhou, W., Zheng, M., Gu, R., *et al.* (2023) STAT3 regulates antiviral immunity by suppressing excessive interferon signaling. *Cell Rep.* **42**, 112806
50. Looyenga, B. D., Hutchings, D., Cherni, I., Kingsley, C., Weiss, G. J., and MacKeigan, J. P. (2012) STAT3 is activated by JAK2 independent of key oncogenic driver mutations in Non-Small cell lung carcinoma. *PLoS One* **7**, e30820
51. Gong, J. H., Maki, G., and Klingemann, H. G. (1994) Characterization of a human cell line (NK-92) with phenotypical and functional characteristics of activated natural killer cells. *Leukemia* **8**, 652–658
52. Deng, L., Liang, H., Xu, M., Yang, X., Burnette, B., Arina, A., *et al.* (2014) STING-dependent cytosolic DNA sensing promotes radiation-induced type I interferon-dependent antitumor immunity in immunogenic tumors. *Immunity* **41**, 843–852
53. Chen, M., Yu, S., van der Sluis, T., Zwager, M. C., Schröder, C. P., van der Veet, B., *et al.* (2024) cGAS-STING pathway expression correlates with genomic instability and immune cell infiltration in breast cancer. *NPJ Breast Cancer* **10**, 1–13

MYC suppresses STING expression

54. Konno, H., Yamauchi, S., Berglund, A., Putney, R. M., Mulé, J. J., and Barber, G. N. (2018) Suppression of STING signaling through epigenetic silencing and missense mutation impedes DNA-damage mediated cytokine production. *Oncogene* **37**, 2037–2051
55. Yu, X., Zhang, L., Shen, J., Zhai, Y., Jiang, Q., Yi, M., *et al.* (2021) The STING phase-separator suppresses innate immune signalling. *Nat. Cell Biol.* **23**, 330–340
56. Mukai, K., Konno, H., Akiba, T., Uemura, T., Waguri, S., Kobayashi, T., *et al.* (2016) Activation of STING requires palmitoylation at the Golgi. *Nat. Commun.* **7**, 11932
57. Ishikawa, H., Ma, Z., and Barber, G. N. (2009) STING regulates intracellular DNA-mediated, type I interferon-dependent innate immunity. *Nature* **461**, 788–792
58. Krenz, B., Gebhardt-wolf, A., Ade, C. P., Gaballa, A., Zender, L., Wolf, E., *et al.* (2021) MYC and MIZ1-dependent vesicular transport of double-strand RNA controls immune evasion in pancreatic ductal adenocarcinoma. *Cancer Res.* **81**, 4242–4256
59. Wolf, E., Gebhardt, A., Kawachi, D., Walz, S., Eyss, B Von, Wagner, N., *et al.* (2013) Miz1 is required to maintain autophagic flux. *Nat. Commun.* **4**, 2535
60. Barré, B., Vigneron, A., and Coqueret, O. (2005) The STAT3 transcription factor is a target for the Myc and riboblastoma proteins on the Cdc25A promoter. *J. Biol. Chem.* **280**, 15673–15681
61. Ramana, C. V., Grammatikakis, N., Chernov, M., Nguyen, H., Goh, K. C., Williams, B. R. G., *et al.* (2000) Regulation of c-myc expression by IFN- γ through Stat1-dependent and -independent pathways. *EMBO J.* **19**, 263–272
62. Hu, J., Sánchez-Rivera, F. J., Wang, Z., Johnson, G. N., Ho, Y jui, Ganesh, K., *et al.* (2023) STING inhibits the reactivation of dormant metastasis in lung adenocarcinoma. *Nature* **616**, 806–813
63. Li, J., Hubisz, M. J., Earlie, E. M., Duran, M. A., Hong, C., Varela, A. A., *et al.* (2023) Non-cell-autonomous cancer progression from chromosomal instability. *Nature* **620**, 1080–1088
64. Hong, C., Schubert, M., Tijhuis, A. E., Requesens, M., Roorda, M., van den Brink, A., *et al.* (2022) cGAS–STING drives the IL-6-dependent survival of chromosomally unstable cancers. *Nature* **607**, 366–373
65. Takaki, T., Millar, R., Hiley, C. T., and Boulton, S. J. (2024) Micronuclei induced by radiation, replication stress, or chromosome segregation errors do not activate cGAS-STING. *Mol. Cell.* **84**, 1–11
66. Sato, Y., and Hayashi, M. T. (2024) Micronucleus is not a potent inducer of the cGAS/STING pathway. *Life Sci Alliance* **7**, 1–18
67. [preprint] Lebre, V., Afshar, N., Davies, L. R., Kujirai, T., Kanellou, A., Tidu, F., *et al.* (2024) A microscopy reporter for cGAMP reveals rare cGAS activation following DNA damage, and a lack of correlation with micronuclear cGAS enrichment. *BioRxiv [Internet]*. <https://doi.org/10.1101/2024.05.13.593978>
68. Kujirai, T., Zierhut, C., Takizawa, Y., Kim, R., Negishi, L., Uruma, N., *et al.* (2020) Structural basis for the inhibition of cGAS by nucleosomes. *Science* **370**, 455–458
69. Flynn, P. J., Koch, P. D., and Mitchison, T. J. (2021) Chromatin bridges, not micronuclei, activate cGAS after drug-induced mitotic errors in human cells. *PNAS* **118**, e2103585118
70. Dunphy, G., Flannery, S. M., Almine, J. F., Connolly, D. J., Paulus, C., Jönsson, K. L., *et al.* (2018) Non-canonical activation of the DNA sensing adaptor STING by ATM and IFI16 mediates NF- κ B signaling after nuclear DNA damage. *Mol. Cell* **71**, 745–760.e5
71. Cerami, E., Gao, J., Dogrusoz, U., Gross, B. E., Sumer, S. O., Aksoy, B. A., *et al.* (2012) The cBio cancer genomics portal: an open platform for exploring multidimensional cancer genomics data. *Cancer Discov.* **2**, 401–404
72. Gao, J., Aksoy, B. A., Dogrusoz, U., Dresdner, G., Gross, B., Sumer, S. O., *et al.* (2013) Integrative analysis of complex cancer genomics and clinical profiles using the cBioPortal. *Sci Signal* **6**, p11
73. Tu, W. B., Shiah, Y. J., Lourenco, C., Mullen, P. J., Dingar, D., Redel, C., *et al.* (2018) MYC interacts with the G9a histone methyltransferase to drive transcriptional repression and tumorigenesis. *Cancer Cell* **34**, 579–595.e8
74. Becht, E., Giraldo, N. A., Lacroix, L., Buttard, B., Elarouci, N., Petitprez, F., *et al.* (2016) Estimating the population abundance of tissue-infiltrating immune and stromal cell populations using gene expression. *Genome Biol.* **17**, 218
75. Llobet, S. G., Bhattacharya, A., Everts, M., Kok, K., Vegt, B Van Der, Fehrmann, R. S. N., *et al.* (2022) An mRNA expression-based signature for oncogene-induced replication stress. *Oncogene* **41**, 1216–1224
76. Cerboni, S., Jeremiah, N., Gentili, M., Gehrmann, U., Conrad, C., Stolzenberg, M. C., *et al.* (2017) Intrinsic antiproliferative activity of the innate sensor STING in T lymphocytes. *J Exp Med* **214**, 1769–1785
77. Gao, L., Zhang, L., Hu, J., Li, F., Shao, Y., Zhao, D., *et al.* (2005) Down-regulation of signal transducer and activator of transcription 3 expression using vector-based small interfering RNAs suppresses growth of human prostate tumor in vivo. *Clin. Cancer Res.* **11**, 6333–6341
78. Ma, L., Deng, X., Wu, M., Zhang, G., and Huang, J. (2014) Down-regulation of miRNA-204 by LMP-1 enhances CDC42 activity and facilitates invasion of EBV-associated nasopharyngeal carcinoma cells. *FEBS Lett.* **588**, 1562–1570
79. Frank, S. R., Schroeder, M., Fernandez, P., Taubert, S., and Amati, B. (2001) Binding of c-Myc to chromatin mediates mitogen-induced acetylation of histone H4 and gene activation. *Genes Dev.* **15**, 2069–2082
80. van den Boom, V., Maat, H., Geugien, M., Rodríguez López, A., Sotoca, A. M., Jaques, J., *et al.* (2016) Non-canonical PRC1.1 targets active genes independent of H3K27me3 and is essential for leukemogenesis. *Cell Rep.* **14**, 332–346
81. Barrilleaux, B. L., Cotterman, R., and Knoepfler, P. S. (2013) Chromatin immunoprecipitation assays for Myc and N-Myc. *Methods Mol. Biol.* **1012**, 117–133
82. Li, L.-C., and Dahiya, R. (2002) MethPrimer: designing primers for methylation PCRs. *Bioinformatics* **18**, 1427–1431